frontiers | Frontiers in Materials

TYPE Original Research
PUBLISHED 19 January 2024
DOI 10.3389/fmats.2024.1330597

OPEN ACCESS

EDITED BY
Zhanyong Zhao,
North University of China, China

REVIEWED BY
Xiaolong Xu,
North University of China, China
Pengcheng Huo,
Taiyuan University of Science and Technology, China
Lizheng Zhang,
Beijing University of Technology, China

*CORRESPONDENCE
Mahesh Naik,
mahesh.naik4144@gmail.com

RECEIVED 31 October 2023
ACCEPTED 02 January 2024
PUBLISHED 19 January 2024

CITATION
Naik M, Pranay V, Thakur DG, Chandel S, Salunkhe S, Pagac M and Abouel Nasr ES (2024), Numerical investigation on effect of different projectile nose shapes on ballistic impact of additively manufactured AlSi10Mg alloy.
Front. Mater. 11:1330597.
doi: 10.3389/fmats.2024.1330597

Numerical investigation on effect of different projectile nose shapes on ballistic impact of additively manufactured AlSi10Mg alloy

Mahesh Naik[1]*, V. Pranay[1], D. G. Thakur[1], Sunil Chandel[1], Sachin Salunkhe[2,3], Marek Pagac[4] and Emad S. Abouel Nasr[5]

[1]Department of Mechanical Engineering, Defence Institute of Advanced Technology (DU), Ministry of Defence, Pune, Maharashtra, India, [2]Department of Biosciences, Saveetha School of Engineering, Saveetha Institute of Medical and Technical Sciences, Chennai, India, [3]Department of Mechanical Engineering, Gazi University Faculty of Engineering, Maltepe, Ankara, Turkey, [4]Department of Machining, Faculty of Mechanical Engineering, Assembly and Engineering Technology, Ostrava-Poruba, Czechia, [5]Department of Industrial Engineering, College of Engineering, King Saud University, Riyadh, Saudi Arabia

In the last few years, due to the superior mechanical qualities of Additive Manufacturing (AM) AlSi10Mg alloy to those of traditional casting process AlSi10Mg alloys, the application of AM technology has significantly increased. The ballistic impact research has a wide range of uses, notably in the mining, construction, spacecraft and defence sectors. This work focuses on analyzing the behavior of different projectile nose shapes on the AlSi10Mg alloy fabricated by AM. There are several projectile nose forms to consider, including blunt, hemispherical, conical, and ogive shapes. The impact of various projectile shapes on the ballistic limit of the additively created AlSi10Mg alloy is carefully examined in this study. All numerical simulations were carried out using LS-DYNA software, and the Johnson-Cook material and damage model were considered to assess the ballistic resistance behavior. The ballistic limit for various projectile shapes is computed using the Jonas-Lambert model, which describes the connection between residual velocity and starting projectile velocity. The results showed that, the ogive-shaped Projectile offers the highest ballistic limit, and the blunt projectile shows the lowest ballistic limit for a 5 mm thin target plate. The ballistic impact phenomenon showed plugging failure for the blunt nose projectile, the formation of plug and small fragments were observed in the case of hemispherical nose projectile, fragmenting failure is observed with radial necking in the case of conical nose projectile and petals are formed at the impacted zone in ogive nose shape projectile. Moreover, the ballistic limit of AM AlSi10Mg alloy was slightly higher compared to the ballistic limit of the die-cast AlSi10Mg alloy for the 7.62 mm AP bullet (core). Therefore, AM AlSi10Mg alloy may have equal or good ballistic properties compared to die-cast AlSi10Mg alloy.

KEYWORDS

AlSi10Mg alloy, additive manufacturing, impact, ballistic limit, FEA

1 Introduction

Equipment and workforces are regularly sent during international operations to distant, extremely volatile locations across the world, which are typically characterized by dysfunction. Small-arm shooting is one of the main threats encountered in these operations (Børvik et al., 2009); thus, choosing the right amount of protection requires a creative approach. Therefore, it is crucial to have the capacity to locally repair, reinforce, or even overhaul the current defensive measures. The production of protective components using additive manufacturing on-site is an undiscovered but practical possibility. There needs to be more research that examines the ballistic resistance of additively generated metal plates in the public domain despite the promise of quickly improving protective structures (Ngo et al., 2018).

The ballistic performance of the materials against rapidly penetrating objects has long been a significant research topic. Composite structures, ceramics, polymers, and metal alloys, such as titanium, steel, and aluminum, are generally preferred in armor designs individually or in combinations. These materials have some advantages over each other according to the usage area. Low-density aluminum alloys are substantially used in applications where weight is a crucial design criterion.

The development of the AlSi10Mg alloy has accelerated significantly in the last few years because of the application of Additive Manufacturing (AM) technologies. This expansion is ascribed to the alloy's improved mechanical qualities compared to those obtained using traditional casting techniques. In the AM process, the specific microstructural characteristics, including grain shape, texture, minimal porosity, and residual stresses, are managed by considering optimized process parameters. Among other metal AM processes, Selective Laser Melting (SLM) stands out with its design flexibility, short production cycle, high geometric accuracy, relatively low production costs, and ability to form suitable microstructures. But non-optimized process parameters can lead to a high density of defects, large grain size, high anisotropy, and stress build-up. Therefore, it is important to study the ballistic impact of AM AlSi10Mg alloy and compared its results with conventionally fabricated AlSi10Mg alloy.

The literature review shows that few studies have been found on the ballistic impact of AM AlSi10Mg alloy, and vast data has been found on the ballistic impact of conventionally fabricated Al alloys. AlSi10Mg alloy was created by Li et al. (Li et al., 2016) using SLM technology, and its fracture behavior and microstructure were examined. The yield and fracture stress for various post-processing techniques were compared. In comparison to other post-processing techniques, it was discovered that the vertical component's yield and fracture stress were greater in the as-built state. The effect of constructed orientation on tensile characteristics of the AlSi10Mg alloy produced by SLM was studied by Rakesh et al. (Ch et al., 2019). They claimed that the constructed orientation had an impact on the tensile qualities, with the vertical component showing higher strength than the horizontal component. On AlSi10Mg alloy created by SLM, Hitzler et al. (Hitzler et al., 2019) conducted fracture toughness studies. According to their research, the fracture toughness of the ordinary bulk material and selectively laser-melted samples was comparable. Through experimental and computational investigations, Kristoffersen et al. (Kristoffersen et al., 2020) examined the ballistic perforation resistance of additively made aluminum plates. AlSi10Mg alloy plates were additively produced on a PBF machine, and their resistance to perforation was evaluated by firing APM2 bullets at various velocities through them. The study compared the effects of AP bullets with and without just the hardcore on the plates. The samples from a block of traditionally die-cast AlSi10Mg alloy with the same chemical makeup as the powder used in 3D printing underwent similar tests. The performance differences in ballistics between die-cast and additive-produced materials were negligible. The investigators concluded that additive-created materials may have ballistic qualities that are on par with or even better than those of conventionally made materials with equal chemical compositions.

Using FEM simulations, Nirmal et al. (Nirmal et al., 2021) investigated the impact behavior of an additively made AlSi10Mg alloy and the ballistic limit of projectiles. The AlSi10Mg that was

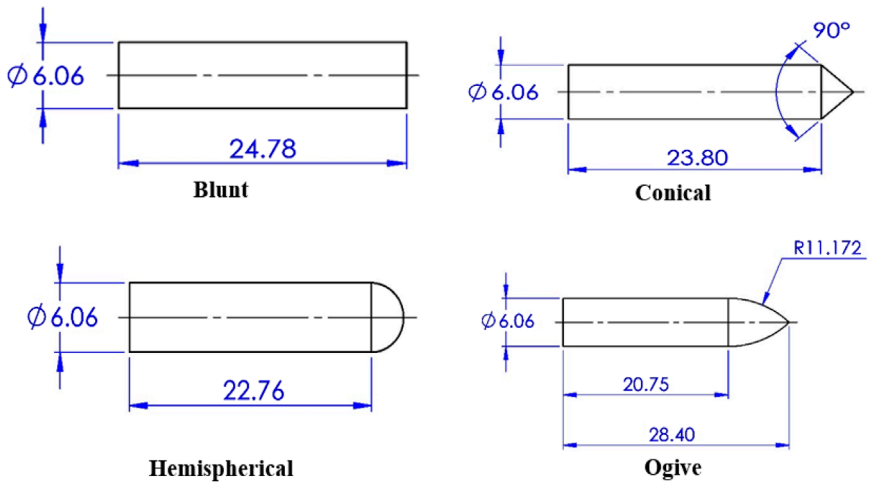

FIGURE 1
2D geometry of different projectile nose shapes.

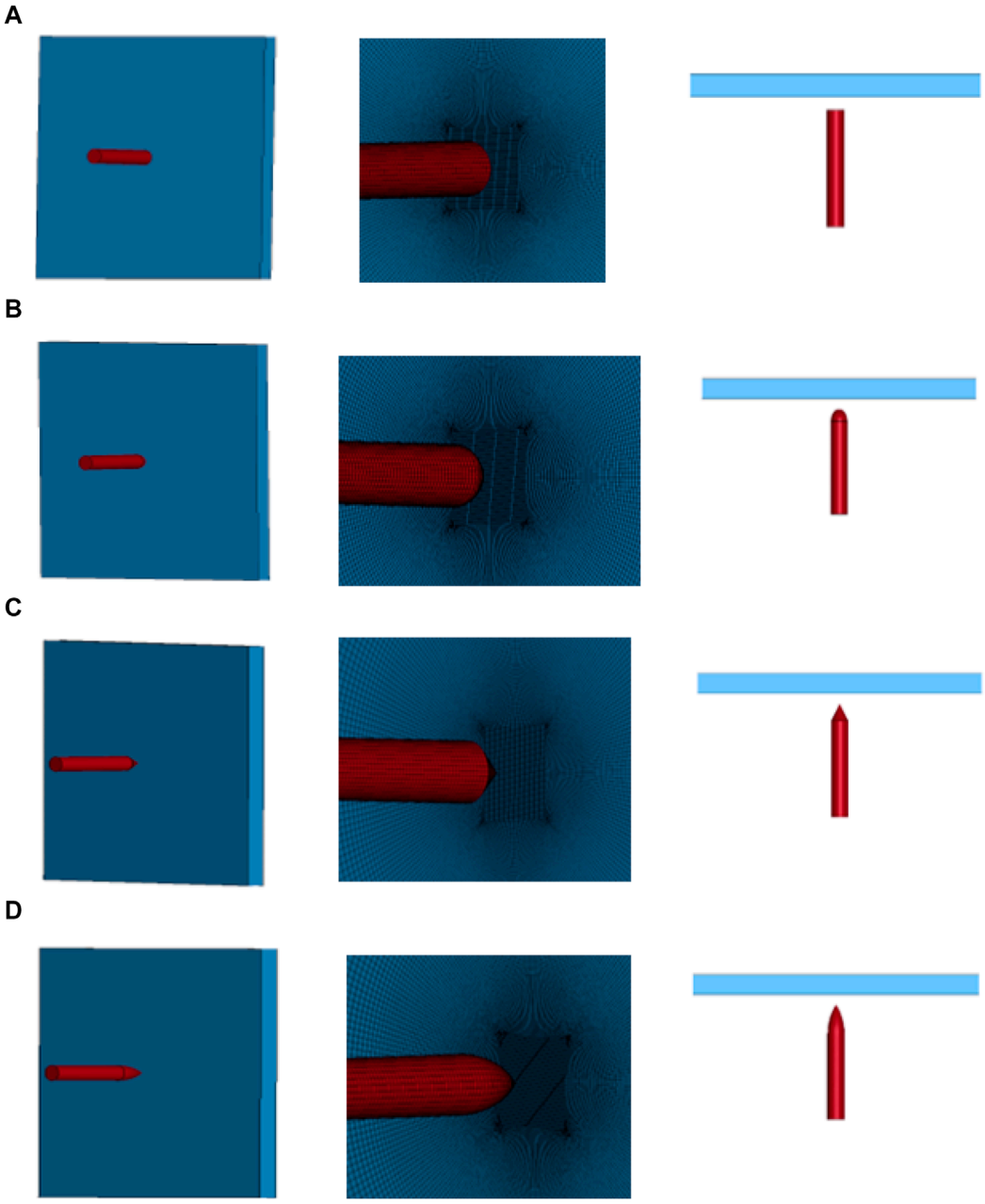

FIGURE 2
Numerical models of target and **(A)** blunt **(B)** hemispherical **(C)** conical **(D)** ogive projectiles.

AM showed plugging and petaling failure upon ballistic hit with hemispherical projectiles, but only plugging failure upon impact with blunt projectiles, it was noted. Hemispherical projectiles were shown to have a larger ballistic limit than blunt projectiles. When Kaya et al. (Oktay et al., 2022) examined the ballistic performance of body-centred lattice structures with different cell heights, they discovered that as the aspect ratio of the unit cell grew, the resistance to penetration improved. The outcomes showed that by optimizing the unit cell height parameter, lattice structures' ballistic performance was improved. *In their investigations into the effects of projectile shape and target thickness, Borvik et al.* (Børvik et al., 2002a; Børvik et al., 2002b) *and Kpenyigba et al.* (Kpenyigba et al., 2013) *concluded that hemispherical projectiles exhibit a higher ballistic limit than blunt and conical projectiles. In comparison, thicker target plates exhibit a higher ballistic limit. Using the Johnson-Cook material and damage model, Gupta et al.* (Gupta et al., 2006; Gupta et al., 2007) *carried out both experimental and computational experiments to illustrate the effect of projectile nose shape on aluminum target plates. In contrast to the effectiveness of hemispherical or ogive-nosed penetrators, Wingrove's* (Wingrove,

TABLE 1 Johnson-Cook material and damage parameters for target and Projectile.

Material model values	AlSi10Mg alloy (Nirmal et al., 2021)	4340-H steel (Segebade et al., 2019)
A	167 MPa	791 MPa
B	396 MPa	510 MPa
C	0.001	0.26
n	0.5510	0.014
m	0.859	1.03
D-1	0	0
D-2	0.873	0
D-3	−0.449	0
D-4	0.00147	0
D-5	0.8	0

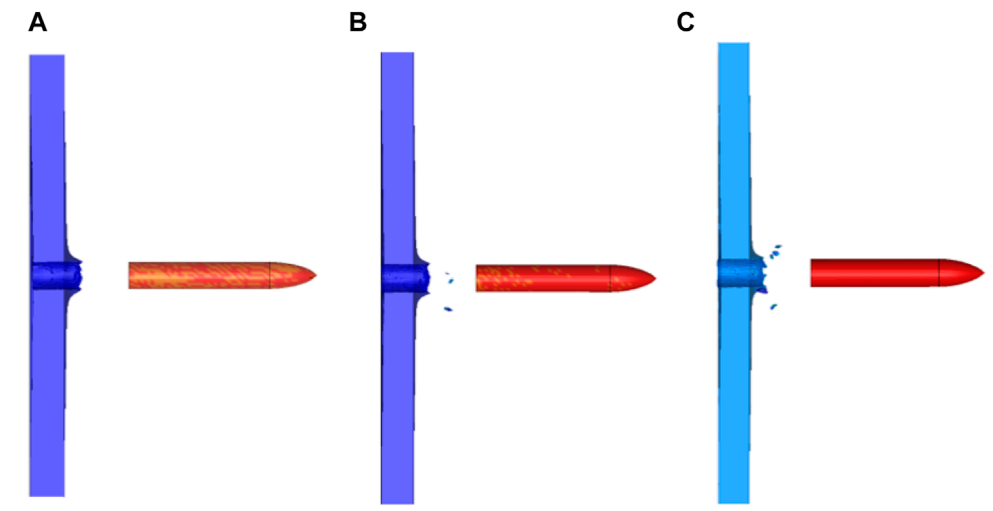

FIGURE 3
Mesh convergence study of the target against Ogive projectile **(A)** 0.35 mm **(B)** 0.25 mm **(C)** 0.15 mm.

1973) *studies on targets made of aluminum alloy found that blunt projectiles may easily pierce the target if the target thickness to projectile diameter ratio is less than one.* Conical projectiles are efficient penetrators, as Othe et al. (Ohte et al., 1982) found. The target's resistance to perforation reduces as the angle of their nose increases. It was discovered that the critical perforation energies of blunt and hemispherical bullets were the same. To avoid mesh distortion and changing contact problems, Camacho and Ortiz (Camacho and Ortiz, 1997) performed finite element simulations of projectile impact. In the case study involving the collision of aluminum plates with conical-nosed projectiles, they discovered a significant connection between the computational and experimental results.

Based on the preceding research, the goal of this work is to simulate the high-speed impact behavior of an additively built AlSi10Mg alloy using the material parameters that are already known. Ballistic impact simulations using blunt, conical, hemispherical, and Ogive projectiles use the Johnson-Cook material and damage model for the additively manufactured AlSi10Mg alloy. The ballistic limit is determined in this study using the Jonas-Lambert equation to establish the link between residual velocity and initial projectile velocity (Børvik et al., 2002b). The empirical model by Lambert and Jonas assumes that the penetrator is a stiff or non-deformable body. The study investigates the impact of several projectile forms on a thin target plate, determining the ballistic limit for each projectile nose type.

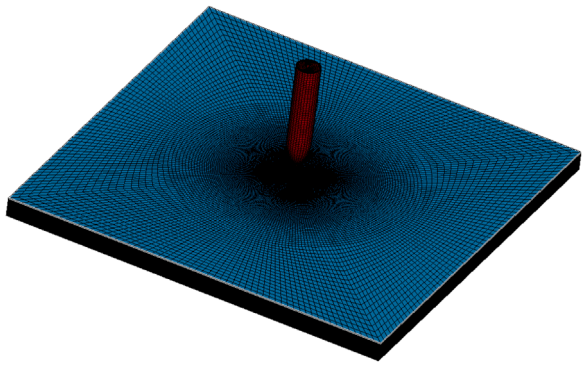

FIGURE 4
7.62 mm AP bullet (core) and AlSi10Mg plate numerical model.

2 Finite element modelling

The numerical analysis of the ballistic impact of additively manufactured AlSi10Mg alloy is carried out in LS-DYNA software. This software is suitable for high-strain rate deformation and is, hence, mostly used for impact analysis. The 3D model of the target and the Projectile is created in LS-DYNA software. The 2D geometry of different projectiles is shown in Figure 1. The geometry of the Projectile having an ogive shape was considered as per the core of a 7.62 mm AP bullet. Since the geometry and mass of the ogival-nosed projectile considered are retained, its diameter is used in creating 3D models of other projectiles with different lengths and nose shapes to maintain constant volume for all projectiles. The 3D model of the target and four different projectiles is shown in Figures 2A–D. The square target of dimensions 100*100*5 mm^3 and projectiles were modelled as deformable bodies. The target was assigned fixed boundary conditions at the periphery. The contact between the Projectile and target was modelled by employing an eroding surface-to-surface contact algorithm with COF 0.2. The Projectile was considered an enslaved person, and the contact surface of the target was the master surface.

3 Materials for target and projectile

The material model is important in getting accurate results of finite element simulations, especially for impact analysis. In the present analysis, the Johnson-Cook material and damage model is considered. Eqs 1–3 represent failure criteria, damage parameters and failure damage. The model allows for isotropic strain hardening, yielding, plastic flow, strain rate effect, and softening brought on by adiabatic heating and damage. The equivalent stress (σ), according to the Johnson-Cook model, is depicted in Eq. 1.

$$\sigma = [A + B\epsilon^n]\left[1 + C\ln\frac{\dot{\epsilon}}{\epsilon_{ref}}\right]\left[1 - \left(\frac{T - T_0}{T_m - T_0}\right)^m\right] \quad (1)$$

where,
A = yield stress at a reference strain rate.
B = strain hardening.n = strain hardening exponent.
ε = strain.
C = strain rate sensitivity.
$\dot{\epsilon}$ = strain rate
ε_{ref} = reference strain rate.
m = temperature exponent.
T = current temperature.
Tm = melting temperature.
T0 = reference temperature.

The equivalent failure strain, as shown in Eq. 2, is affected by the analysis of the stress triaxiality, strain rate, and temperature.

$$\varepsilon_f = \left[D_1 + D_2 e^{D_3\sigma^*}\right][1 + D_4 \ln\dot{\varepsilon}]\left[1 + D_5\frac{T - T_0}{T_m - T_0}\right] \quad (2)$$

where D_1–D_5 are the empirical coefficients of the materials.

Damage evolution is zero while the material is exposed to elastic deformation. After the cumulative plastic strain reaches a certain threshold, degradation begins to take place. Eq. 3 is an illustration of Johnson Cook's damage evolution.

$$\dot{D} = \begin{cases} 0 & \varepsilon < p_d \\ \dfrac{D_c}{\varepsilon_f - p_d}\dot{\varepsilon}, & \varepsilon \geq p_d \end{cases} \quad (3)$$

p_d represents the damage threshold, fracture strain is represented by ε_f, and Dc represents the critical damage parameter. Elements with

TABLE 2 Residual velocities after penetrations.

Initial-velocity (m/s)	Residual-velocity (m/s) (Kristoffersen et al., 2020)	Residual-velocity (m/s) [numerical results]	Numerical error (%)
225	0	0	0
340	257	252	1.94
445	384	380	1.04
515	465	460	1.07
585	530	525	0.94
665	620	614	0.97
725	693	687	0.86

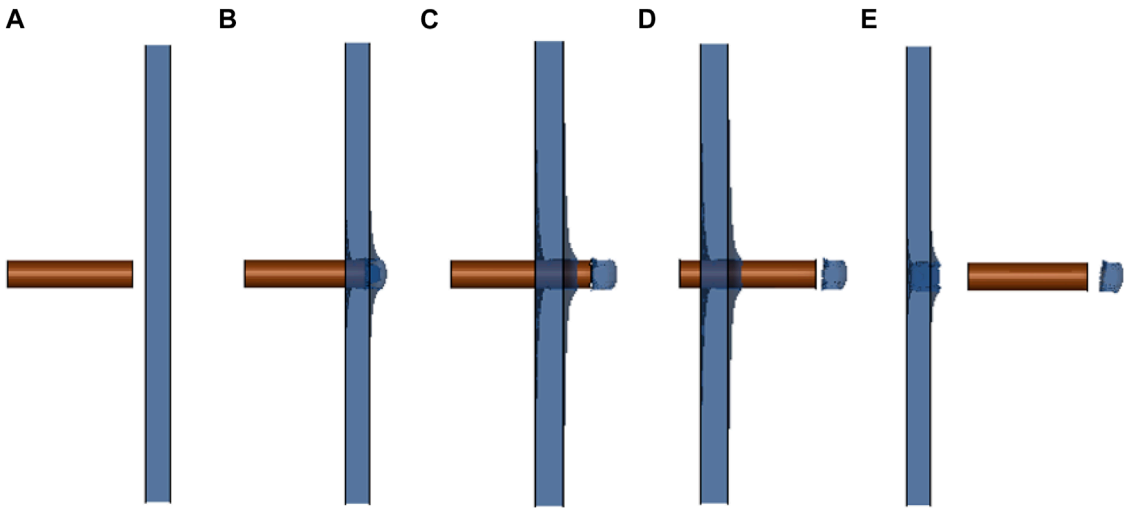

FIGURE 5
Penetration and perforation of projectile (blunt) with velocity of 250 m/s **(A)** 0 μs **(B)** 32 μs **(C)** 64 μs **(D)** 129 μs **(E)** 226 μs time interval.

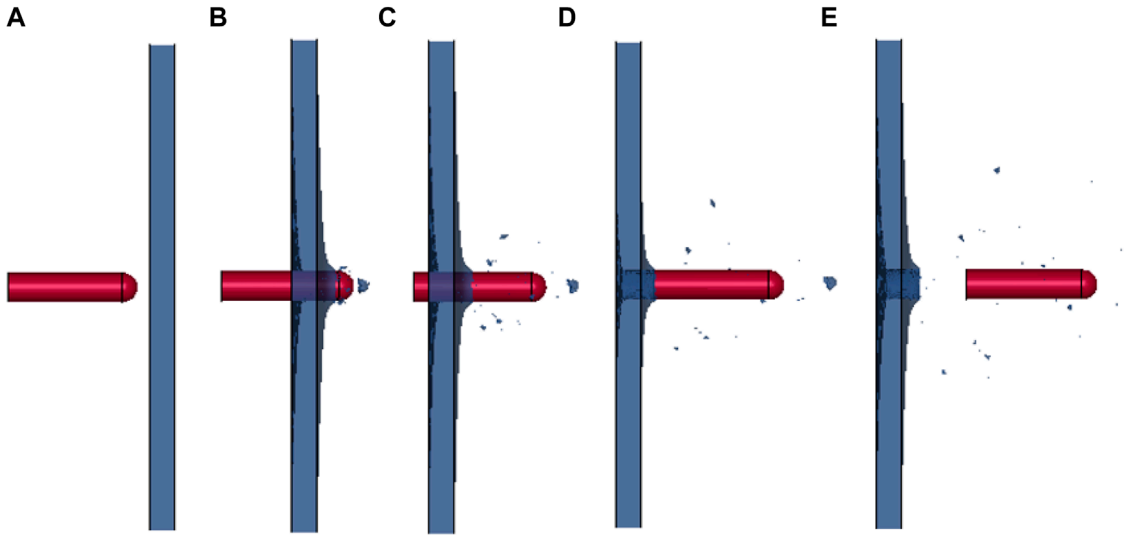

FIGURE 6
Penetration and perforation of projectile (hemispherical) with velocity of 250 m/s **(A)** 0 μs **(B)** 80 μs **(C)** 161 μs **(D)** 242 μs **(E)** 323 μs time interval.

nodes and meshes were used to build solid bodies, and each element has a unique damage value. The linked element is removed from the simulation when $\dot{D}$ reaches a value of 1.

In the present investigation, the target material was considered additively manufactured AlSi10Mg alloy fabricated through the SLM technique, and the projectile material was selected 4340-H steel. The Johnson-Cook material and damage parameters for AlSi10Mg alloy (Segebade et al., 2019; Oktay et al., 2022) and 4340-H steel (Fras et al., 2015) were taken from available literature and represented in Table 1. As the damage parameters were not considered for steel, the 0.3 value was assigned to the "EFFEPS" parameter in the "MAT_ADD_EROSION" section of the model. The Equation of state function (Mie Grüneisen) for the target material (Fras et al., 2015) and the Projectile (Elshenawy and Li, 2013) was considered from the literature.

4 Mesh convergence study

The mesh sensitivity in the target was investigated by changing the element size in the impact zone to 0.15 mm, 0.25 mm, and 0.35 mm, equivalent to 33, 20, and 15 elements at the target thickness. On a target that was 5 mm thick, the ogive projectile struck perpendicular to the surface with an incidence velocity of

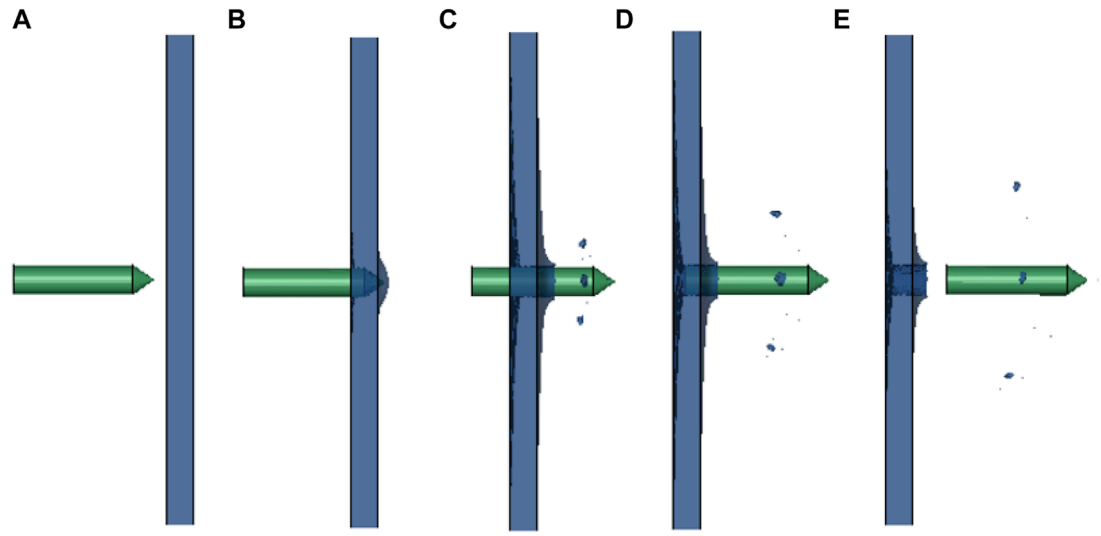

FIGURE 7
Penetration and perforation of Projectile (conical) with 250 m/s velocity **(A)** 0 μs **(B)** 32 μs **(C)** 96 μs **(D)** 145 μs **(E)** 193 μs time interval.

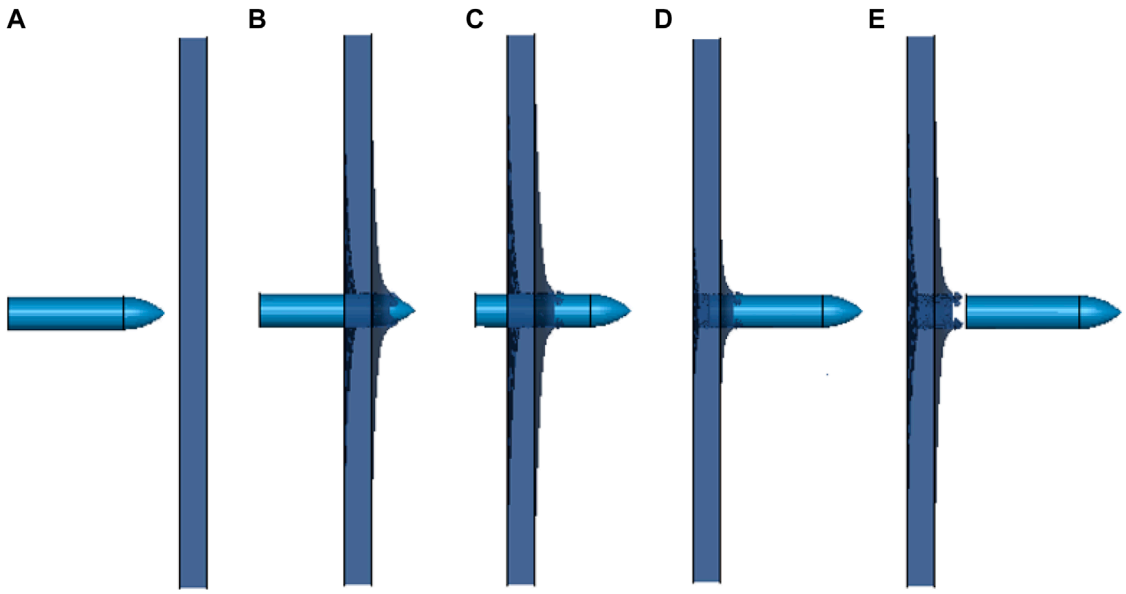

FIGURE 8
Penetration and perforation of Projectile (ogive) with 250 m/s velocity **(A)** 0 μs **(B)** 32 μs **(C)** 96 μs **(D)** 145 μs **(E)** 193 μs time interval.

663.5 m/s. The resulting residual velocities were 622 m/s, 619 m/s, and 617 m/s, respectively. Regarding residual velocity, the target's mesh sensitivity was minimal. However, different mesh sizes significantly affected the mode of failure (see Figures 3A–C). The target's failure mechanism closely matched the failure pattern seen in the experimental investigation (Kristoffersen et al., 2020) with a 0.15 mm element size. As a result, 0.15 mm was chosen as the element size for all simulations. The element size was somewhat raised outside of the impact zone while the aspect ratio remained constant.

5 Numerical model validation

The validation of the FEA model was done by comparing the FEA results with experimental results (Kristoffersen et al., 2020). The core of a 7.62 mm AP bullet of 4340-H steel material was perforated in additively manufactured AlSi10Mg alloy plates with the size of 100*100*5 mm^3. The initial velocities of the projectile were in the range of 200 m/s–725 m/s. The numerical model of projectile and target is shown in Figure 4.

10.3389/fmats.2024.1330597

TABLE 3 Impact velocity vs. residual velocity projectile nose shapes.

Blunt-projectile		Hemispherical-projectile		Conical-projectile		Ogive-projectile	
Impact Velocity (m/s)	Residual Velocity (m/s)	Impact Velocity (m/s)	Residual Velocity (m/s)	Impact Velocity (m/s)	Residual Velocity (m/s)	Impact Velocity (m/s)	Residual Velocity (m/s)
225	129	250	126	275	156	250	95
250	171	275	175	300	198	275	157
275	205	300	213	325	236	300	196
300	234	325	247	350	270	325	231
325	261	350	279	375	301	350	265
350	287	375	309	400	332	375	296

6 Result and discussion

6.1 Validation study

The FEA results are validated with the experimental results available in the literature (Kristoffersen et al., 2020). The values of residual velocities of 7.62 mm AP bullets (core) obtained from FEA analysis were compared with the experimental residual velocities values fitted by the Recht-Ipson model (Kristoffersen et al., 2020). The comparison is shown in Table 2 with error values. The values were in good agreement with experimental values, including Johnson-Cook material model parameters.

6.2 Ballistic impact on AlSi10Mg alloy plate

The objective of this research is to carry out a numerical investigation of the ballistic impact phenomena on an alloy made of AlSi10Mg using additive manufacturing. The purpose of the study is to assess the ballistic limit of projectiles with different types of nose forms, such as blunt, hemispherical, conical, and ogive. These projectiles were fired at a thin target plate at speeds between 150 m/s and 450 m/s. The target plate exhibits stretching and ricocheting after impact when the projectile's initial velocity is lower than its total penetration velocities. The plugging failure that occurred after the discharge of a blunt projectile with an initial velocity of 250 m/s is shown in Figure 5. After the bullet strikes the target plate, there are noticeable radial and circumferential strains created. The Projectile's motion, which moves the target plate in the direction of its trajectory and generates a bending force, results in the deformation. When the tension eventually exceeds the target plate's tensile strength, a plug separates from the plate.

Figure 6 shows pictures taken along the travel path of the hemispherical Projectile as it is fired at a velocity of 250 m/s towards a thin target plate. When the target plate reaches its maximal strength point, it punctures, causing the hemispherical projectile's velocity to drop dramatically. The failure of the target was caused by ductile hole expansion, the formation of a small plug, and the production of fragments owing to fractures along their back edges.

Figure 7 depicts many examples of a conical projectile striking a target plate at 250 m/s. A small fragment failure occurs as the conical-shaped projectile enters the target, which is attributable to radial necking generated by radial stress. The projectile's 90° nose angle induced catastrophic failure in the target as a result of ductile hole expansion and shear plugging.

Figure 8 depicts the snapshot of an ogive projectile impacting a target plate with a velocity of 250 m/s at various times. Figure 8E depicts the formation of petals in the affected zone following the fracture of the target plate.

7 Evaluation of ballistic limit

Several computational and empirical models exist to estimate the ballistic limit. Lambert and Jonas provided one such empirical model. The penetrator is modelled as a non-deformable or stiff body in this model. The following is the relationship between striking velocity (V_s), residual velocity (V_r), and ballistic limit velocity (V_{bl}).

$$V_r = \begin{cases} 0, & 0 \le V_S \ge V_{bl} \\ \beta(V_S{}^p - V_{bl}{}^p)^{\frac{1}{p}}, & V_S \ge V_{bl} \end{cases} \quad (4)$$

Where β and p are model constants.

A typical curve fitting approach is used in current work to determine ballistic limit and Lambert-Jonas model parameters. To fit numerical data to the Lambert-Jonas model, the beginning projectile and residual velocities of blunt, hemispherical, conical, and ogive projectiles from Table 3 were considered.

The curve fit values of the ballistic limit (V_{bl}) and the model constants (β and p) obtained from Eq. 4 for the thin target plate formed of AM AlSi10Mg alloy are as follows.

(a) Blunt projectile
V_{bl} = 202.048 m/s, p = 2.99, β = 0.8807
(b) Hemispherical Projectile
V_{bl} = 225.63 m/s, p = 2.3934, β = 0.9539
(c) Conical Projectile
V_{bl} = 233.87 m/s, p = 2.1973, β = 0.9809

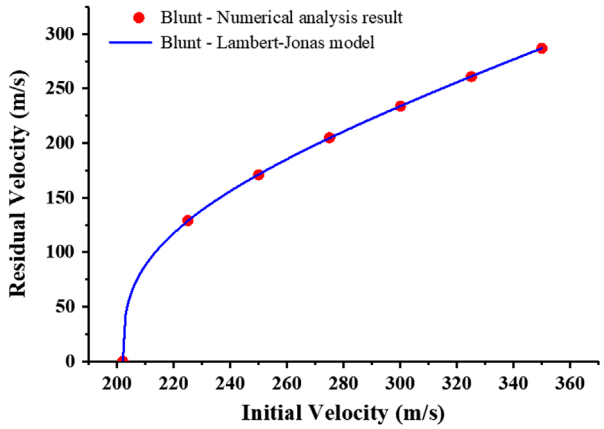

FIGURE 9
Residual vs. initial velocity of Projectile (blunt) for thin target plate.

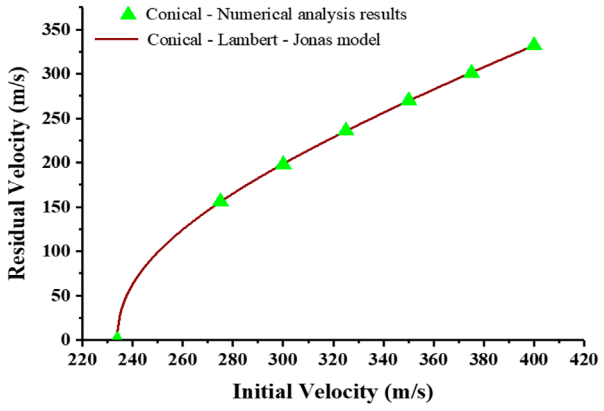

FIGURE 11
Residual vs. initial velocity of Projectile (conical) for thin target plate.

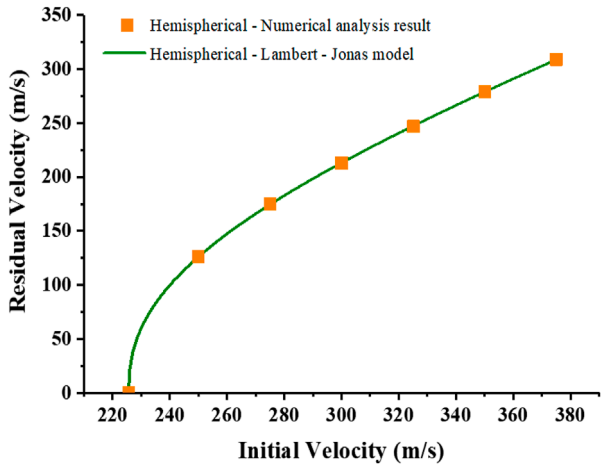

FIGURE 10
Residual vs. initial velocity of Projectile (hemispherical) for thin target plate.

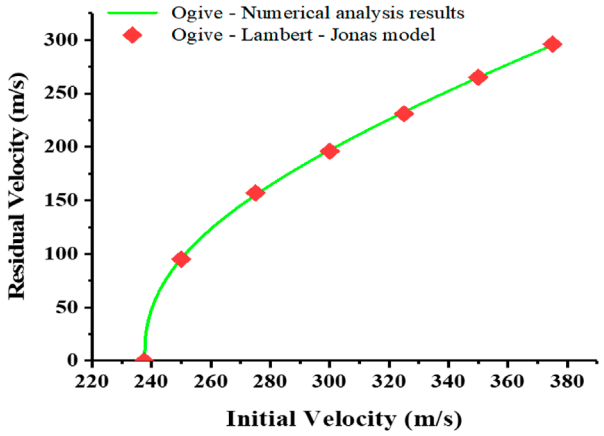

FIGURE 12
Residual vs. initial velocity of Projectile (ogive) for thin target plate.

(d) Ogive projectile
V_{bl} = 237.5280 m/s, p = 2.4210, β = 0.9289

Figure 9, Figure 10, Figure 11, and Figure 12 show the curve fitting for the AM AlSi10Mg alloy thin target plate's blunt, hemispherical, conical, and ogive projectiles. The regression curve was created using seven data points and the non-linear least square approach to determine the ballistic limit and Lambert-Jonas model parameters. The regression curves are near 99.8% of the data points. Furthermore, the accuracy of the Lambert-Jonas model and the Recht-Ipson model is comparable (Ben-Dor et al., 2002), suggesting that ballistic limit velocities and Lambert-Jonas parameters obtained using the least-square technique are well-suited.

Further, the ballistic limit of the blunt Projectile was found to be minimal compared to other projectile nose shapes because the target thickness (5 mm) to projectile diameter (6.06 mm) ratio is less than one, which resulted in easy perforation of the target (Wingrove, 1973). Also, the ballistic limit of the conical Projectile was higher compared to hemispherical and shape projectiles, which was in line with the results found in the literature (Rodriguez-Millán et al., 2014; Senthil et al., 2018; Nirmal et al., 2021). The ogive-shaped nose projectile requires more energy to perforate the target at a higher velocity, which has resulted in a higher ballistic limit, and the residual velocity of the ogive projectile was less compared to another projectile (Raguraman et al., 2008).

8 Conclusion

The numerical examinations of ballistic impact on additively made AlSi10Mg alloy with variable projectile nose shapes have been done in this paper. The impact of diverse projectile shapes with varied velocity and ballistic limits has been explored. For the additively created AlSi10Mg alloy from the literature, the Johnson-Cook material model and damage model were used. Based on the findings of the above investigation, the following conclusions were reached.

- The numerically investigated ballistic impact results of AM AlSi10Mg alloy were compared with the experimental results available in literature by considering the ogive shape of the projectile. It was observed that the percent error in ballistic limit was between 0.8% and 2%.
- The ballistic impact phenomenon showed plugging failure for the blunt nose projectile; the formation of plug and small fragments were observed in the case of hemispherical nose projectile, fragmenting failure is observed with radial necking in the case of conical nose projectile and petals are formed at the impacted zone in ogive nose shape projectile.
- The ballistic limit and associated parameters for projectiles with varied nose shapes are determined using Jonas and Lambert's model. In contrast to other projectile nose shapes, the ballistic limit of an ogive nose shape projectile is found to be the highest and the ballistic limit of a blunt nose shape projectile is found to be lowest for AM AlSi10Mg alloy with a thickness of 5 mm.
- The ballistic limit of ogive nose shape projectile is found to be higher by 14.93%, 5% and 1.5% compared to blunt, conical and ogive nose shape projectile, respectively.
- The ballistic limit of additively manufactured AlSi10Mg alloy (238 m/s) was slightly higher compared to the ballistic limit of the die-cast AlSi10Mg alloy (223 m/s) (Kristoffersen et al., 2020) for the 7.62 mm AP bullet (core). Therefore, additively manufactured AlSi10Mg alloy may have equal or good ballistic properties compared to die-cast AlSi10Mg alloy.

Data availability statement

The original contributions presented in the study are included in the article/Supplementary material, further inquiries can be directed to the corresponding author.

Author contributions

MN: Conceptualization, Data curation, Investigation, Methodology, Project administration, Resources, Writing–original draft, Writing–review and editing. VP: Data curation, Formal Analysis, Methodology, Software, Visualization, Writing–review and editing. DT: Data curation, Funding acquisition, Investigation, Project administration, Resources, Software, Supervision, Validation, Writing–review and editing. SC: Data curation, Investigation, Project administration, Resources, Writing–review and editing. SS: Conceptualization, Methodology, Project administration, Resources, Writing–review and editing. MP: Funding acquisition, Project administration, Software, Supervision, Writing–review and editing. EA: Funding acquisition, Methodology, Project administration, Software, Writing–review and editing.

Funding

The author(s) declare financial support was received for the research, authorship, and/or publication of this article. The authors extend their appreciation to King Saud University for funding this work through Researchers Supporting Project number (RSP 2024R164), King Saud University, Riyadh, Saudi Arabia. In addition, this paper was completed in association with the project "Materials and Technologies for Sustainable Development—MATUR," registration no. CZ.02.01.01/00/22_008/0004631 financed by the Structural Funds of European Union project.

Conflict of interest

The authors declare that the research was conducted in the absence of any commercial or financial relationships that could be construed as a potential conflict of interest.

Publisher's note

All claims expressed in this article are solely those of the authors and do not necessarily represent those of their affiliated organizations, or those of the publisher, the editors and the reviewers. Any product that may be evaluated in this article, or claim that may be made by its manufacturer, is not guaranteed or endorsed by the publisher.

References

Ben-Dor, G., Dubinsky, A., and Elperin, T. (2002). On the Lambert–Jonas approximation for ballistic impact. *Mech. Res. Commun.* 29 (23), 137–139. doi:10.1016/s0093-6413(02)00246-x

Børvik, T., Dey, S., and Clausen, A. H. (2009). Perforation resistance of five different high-strength steel plates subjected to small-arms projectiles. *Int. J. Impact Eng.* 36 (7), 948–964. doi:10.1016/j.ijimpeng.2008.12.003

Børvik, T., Hopperstad, O. S., Berstad, T., and Langseth, M. (2002b). Perforation of 12 mm thick steel plates by 20 mm diameter projectiles with flat, hemispherical and conical noses: part II: numerical simulations. *Int. J. impact Eng.* 27 (1), 37–64. doi:10.1016/s0734-743x(01)00035-5

Børvik, T., Langseth, M., Hopperstad, O. S., and Malo, K. A. (2002a). Perforation of 12 mm thick steel plates by 20 mm diameter projectiles with flat, hemispherical and conical noses: Part I: experimental study. *Int. J. impact Eng.* 27 (1), 19–35. doi:10.1016/s0734-743x(01)00034-3

Camacho, G. T., and Ortiz, M. (1997). Adaptive Lagrangian modelling of ballistic penetration of metallic targets. *Comput. methods Appl. Mech. Eng.* 142 (34), 269–301. doi:10.1016/s0045-7825(96)01134-6

Ch, S. R., Raja, A., Nadig, P., Jayaganthan, R., and Vasa, N. J. (2019). Influence of working environment and built orientation on the tensile properties of selective laser melted AlSi10Mg alloy. *Mater. Sci. Eng. A* 750, 141–151. doi:10.1016/j.msea.2019.01.103

Elshenawy, T., and Li, Q. M. (2013). Influences of target strength and confinement on the penetration depth of an oil well perforator. *Int. J. Impact Eng.* 54, 130–137. doi:10.1016/j.ijimpeng.2012.10.010

Fras, T., Colard, L., and Pawlowski, P. (2015). Perforation of aluminum plates by fragment simulating projectiles (FSP). *Int. J. Multiphysics* 9 (3), 267–286. doi:10.1260/1750-9548.9.3.267

Gupta, N. K., Iqbal, M. A., and Sekhon, G. S. (2006). Experimental and numerical studies on the behavior of thin aluminum plates subjected to impact by blunt- and hemispherical-nosed projectiles. *Int. J. Impact Eng.* 32 (12), 1921–1944. doi:10.1016/j.ijimpeng.2005.06.007

Gupta, N. K., Iqbal, M. A., and Sekhon, G. S. (2007). Effect of projectile nose shape, impact velocity and target thickness on deformation behavior of aluminum plates. *Int. J. Solids Struct.* 44 (10), 3411–3439. doi:10.1016/j.ijsolstr.2006.09.034

Hitzler, L., Hirsch, J., Schanz, J., Heine, B., Merkel, M., Hall, W., et al. (2019). Fracture toughness of selective laser melted AlSi10Mg. *Proc. Institution Mech. Eng. Part L J. Mater. Des. Appl.* 233 (4), 615–621. doi:10.1177/1464420716687337

Kpenyigba, K. M., Jankowiak, T., Rusinek, A., and Pesci, R. (2013). Influence of projectile shape on dynamic behavior of steel sheet subjected to impact and perforation. *Thin-Walled Struct.* 65, 93–104. doi:10.1016/j.tws.2013.01.003

Kristoffersen, M., Costas, M., Koenis, T., Brøtan, V., Paulsen, C. O., and Børvik, T. (2020). On the ballistic perforation resistance of additive manufactured AlSi10Mg aluminium plates. *Int. J. Impact Eng.* 137, 103476. doi:10.1016/j.ijimpeng.2019.103476

Li, W., Li, S., Liu, J., Zhang, A., Zhou, Y., Wei, Q., et al. (2016). Effect of heat treatment on AlSi10Mg alloy fabricated by selective laser melting: microstructure evolution, mechanical properties and fracture mechanism. *Mater. Sci. Eng. A* 663, 116–125. doi:10.1016/j.msea.2016.03.088

Ngo, T. D., Kashani, A., Imbalzano, G., Nguyen, K. T., and Hui, D. (2018). Additive manufacturing (3D printing): a review of materials, methods, applications and challenges. *Compos. Part B Eng.* 143, 172–196. doi:10.1016/j.compositesb.2018.02.012

Nirmal, R. R., Patnaik, B. S., and Jayaganthan, R. (2021). FEM simulation of high-speed impact behaviour of additively manufactured AlSi10Mg alloy. *J. Dyn. Behav. Mater.* 7, 469–484. doi:10.1007/s40870-020-00285-1

Ohte, S., Yoshizawa, H., Chiba, N., and Shida, S. (1982). Impact strength of steel plates struck by projectiles: evaluation formula for critical fracture energy of steel plate. *Bull. JSME* 25 (206), 1226–1231. doi:10.1299/jsme1958.25.1226

Oktay, K. A., Hafizoğlu, H., and Babacan, N. (2022). Effect of unit cell height on the ballistic performance of the body-centered lattice structures. *Int. J. Innovative Eng. Appl.* 6 (1), 30–44.

Raguraman, M., Deb, A., Gupta, N. K., and Kharat, D. K. (2008). Numerical simulation of projectile impact on mild steel armour platesusing LS-DYNA, Part II: parametric studies. *Def. Sci. J.* 58 (4), 573–581. doi:10.14429/dsj.58.1679

Rodriguez-Millán, M., Vaz-Romero, A., Rusinek, A., Rodríguez-Martínez, J. A., and Arias, A. (2014). Experimental study on the perforation process of 5754-H111 and 6082-T6 aluminium plates subjected to normal impact by conical, hemispherical and blunt projectiles. *Exp. Mech.* 54, 729–742. doi:10.1007/s11340-013-9829-z

Segebade, E., Gerstenmeyer, M., Dietrich, S., Zanger, F., and Schulze, V. (2019). Influence of anisotropy of additively manufactured AlSi10Mg parts on chip formation during orthogonal cutting. *Procedia CIRP* 82, 113–118. doi:10.1016/j.procir.2019.04.043

Senthil, K., Iqbal, M. A., Arindam, B., Mittal, R., and Gupta, N. K. (2018). Ballistic resistance of 2024 aluminium plates against hemispherical, sphere and blunt nose projectiles. *Thin-Walled Struct.* 126, 94–105. doi:10.1016/j.tws.2017.02.028

Wingrove, A. L. (1973). The influence of projectile geometry on adiabatic shear and target failure. *Metall. Trans.* 4, 1829–1833. doi:10.1007/bf02665409